

## Article

# Enhancement and Mechanism of Rhodamine B Decomposition in Cavitation-Assisted Plasma Treatment Combined with Fenton Reactions

Yifan Xu <sup>1,\*</sup>, Sergey Komarov <sup>2</sup>, Takuya Yamamoto <sup>2</sup> and Takaaki Kutsuzawa <sup>2</sup><sup>1</sup> Graduate School of Environmental Studies, Tohoku University, Sendai 980-8577, Japan<sup>2</sup> Department of Metallurgy, Materials Science and Materials Processing, Tohoku University, Sendai 980-8577, Japan

\* Correspondence: xu.yifan.p3@dc.tohoku.ac.jp

**Abstract:** In our previous study, a novel method combining underwater high-voltage plasma discharge with acoustic cavitation (ACAP) was developed and implemented using rhodamine B (*RhB*) as a model organic pollutant. Results revealed that injecting argon gas into the ACAP reactor positively influences *RhB* decomposition efficiency, but there is still further potential for improvement. The aim of this study was therefore to further improve the efficiency of the ACAP process through Fenton reactions. Two options for ferrous ion supply were considered: the addition of FeCl<sub>2</sub> or the dissolution of iron from ACAP reactor steel parts into the *RhB*-containing solution. The results revealed that the degradation efficiency is increased by 20% due to the Fenton reactions when the concentration of ferrous ions reaches an optimal value. Lower pH was found to be desirable for the effect of Fenton reactions. Based on measurements using high performance liquid chromatography, a plausible mechanism of *RhB* degradation by the ACAP process assisted by Fenton reactions is additionally proposed and discussed.

**Keywords:** rhodamine B (*RhB*) decomposition; Fenton reactions; acoustic cavitation; underwater plasma



**Citation:** Xu, Y.; Komarov, S.; Yamamoto, T.; Kutsuzawa, T. Enhancement and Mechanism of Rhodamine B Decomposition in Cavitation-Assisted Plasma Treatment Combined with Fenton Reactions. *Catalysts* **2022**, *12*, 1491. <https://doi.org/10.3390/catal12121491>

Academic Editor: Sergey Nikitenko

Received: 26 September 2022

Accepted: 18 November 2022

Published: 22 November 2022

**Publisher's Note:** MDPI stays neutral with regard to jurisdictional claims in published maps and institutional affiliations.



**Copyright:** © 2022 by the authors. Licensee MDPI, Basel, Switzerland. This article is an open access article distributed under the terms and conditions of the Creative Commons Attribution (CC BY) license (<https://creativecommons.org/licenses/by/4.0/>).

## 1. Introduction

Clean water is a vital resource for both animal and human life. Growing populations and industrialization have led to a shortage of clean water in many countries. At present, a wide variety of methods exists worldwide to purify water, including chemical, physical, and biological methods of treatment. Recently, much attention has been placed on physical treatment methods to purify water to meet growing demand [1]. The attractiveness of these methods lies in their ability to eliminate or greatly reduce the use of chemicals in comparison with chemical water treatment methods. It should be noted that the use of chemicals in water purification is greatly restricted in areas such as food processing, medical applications, and drinking water. Physical methods of water purification have gained wide acceptance in the treatment of wastewater containing organic pollutants that are difficult to decompose. Physical methods lower wastewater treatment costs and minimize by-products; hence, they are environmentally friendly. Underwater plasma, ultrasound, and UV irradiation, as well as their combinations, have been proposed [2–4] for the highly efficient treatment of wastewater.

In the recent past, advanced oxidation processes (AOPs) have been implemented as innovative tools for treating wastewater [5]. Introducing radiative, electrical, or chemical energy and catalysts in the reactors can improve the generation of highly reactive radicals that can chemically attack and degrade pollutant molecules [6]. Electrical plasma discharge has proved to be highly efficient in the removal of organic pollutants, with great environmental compatibility. It is associated with extreme physical conditions capable of generating highly

reactive radicals. However, plasma generation in water presents challenges due to the high breakdown voltage required. Additionally, pollutants in water may increase the ionic component of water electrical conductivity, hence making it difficult for breakdown to occur. Ultrasound irradiation generates acoustic cavitation, a physical phenomenon including nucleation, growth, and implosion of gas- or vapor-filled cavities. This cavitation results in the creation of high pressure and temperature hot spots, where a great quantity of highly reactive radicals is generated. However, ultrasonic irradiation-based wastewater treatment has limitations, because the acoustic cavitation zone is restricted in size due to the significant attenuation of ultrasonic wave energy that occurs with the distance traveled from the ultrasonic source to the cavitation zone [7].

In our previous research, we proposed a novel technique for wastewater processing: acoustic cavitation-assisted plasma (ACAP). This technique combines high-voltage pulse discharge and acoustic cavitation [8,9]. In the next step, it was shown that the use of gas injection in the ACAP reactor offers a promising improvement in the process efficiency, which is especially pronounced when argon or oxygen is injected at higher flow rates. This is achieved through the dissolution of gas introduced into the solution, which results in the reduction of the required breakdown voltage and improvement in plasma and cavitation generation [10].

Fenton reagents ( $\text{Fe}^{2+}/\text{H}_2\text{O}_2$  combined) have received wide recognition as powerful oxidants with focused applications in dyed wastewater treatment [11]. Reactions between peroxides (commonly hydrogen peroxide ( $\text{H}_2\text{O}_2$ )) and iron ions, generally known as Fenton or Fenton-related reactions, form reactive oxygen species that act to oxidize both organic and inorganic compounds [12]. In recent research, the synergic effect of Fenton reactions in advanced oxidation processes (AOPs) has been explored, aimed at improving organic pollutant removal [13]. Typically, Fenton reagents such as hydrogen peroxide and ferrous salts are added to the reactor. However, when acoustic cavitation and plasma discharge are used for wastewater treatment, hydrogen peroxide is produced in water as a by-product. Ferrous ions can additionally be supplied to the reaction system from metal parts of the equipment used for the treatment. Typical examples of such parts are the ultrasound sonotrode, the electrode, and the container when made of steel or iron. This approach may provide an advantageous, environment-friendly way to enhance treatment efficiency without the use of additional chemicals.

Based on the above, the goal of this study was to investigate the effects of Fenton reactions on the efficiency of rhodamine B degradation when its aqueous solution was treated in the ACAP reactor, which combines acoustic cavitation, high-voltage plasma discharge, and gas (argon) injection. The selection of argon for gas injection was based on the results of our previous studies [9,10], which revealed that argon injection enhances *RhB* decomposition efficiency significantly. However, even in the current case, it was difficult to achieve adequately high decomposition efficiency in a short treatment time. In the present study, the contribution of Fenton reactions to rhodamine B degradation in the ACAP process was investigated under various concentrations of  $\text{Fe}^{2+}$  ions and pH values. The improvement in the effect of Fenton reactions is discussed on the basis of our previously research. The following experimental section introduces the equipment and ideas.

## 2. Experimental

### 2.1. Experimental Setup

Rhodamine B (Wako Pure Chemical, Osaka, Japan) (hereinafter *RhB*) was used as a model water pollutant in the present experiments. Ferrous chloride,  $\text{FeCl}_2$  (99%, Kojundo Chemical Laboratory, Tokyo, Japan), was used as a source of  $\text{Fe}^{2+}$  ions. Ammonium molybdate, potassium iodide, and phthalic acid were purchased from Wako Pure Chemical, Japan, and were used for preliminary treatment of  $\text{H}_2\text{O}_2$ -containing samples before measurements of  $\text{H}_2\text{O}_2$  concentration. Potassium iodide reacts with hydrogen peroxide when ammonium molybdate and vanillin acid are present, yielding iodovanillic acid as detected by UV absorption at 352 nm [14].

Details of the experimental setup have been reported in our previous papers [9,10]. Therefore, only a brief explanation on the setup will be given here. The three main parts of the ACAP reactor were a cylindrical ultrasound sonotrode of 24 mm in radius, one part of which was made of ceramic and the other of titanium or stainless steel (SUS304); the second was a needle-shaped high voltage electrode made of 1 mm tungsten wire; and the third was a cylindrical vessel (diameter 130 mm, height 300 mm) made of acrylic resin. The sonotrode was screwed into a piezoceramic transducer powered by an ultrasonic generator (WS-1200-28, Honda Electronics, Toyohashi, Japan) with adjustable output power in order to transmit ultrasound vibrations into the aqueous *RhB* solution at a frequency of 20 kHz. The vibration amplitude of the sonotrode tip was set to 36  $\mu\text{m}$  (p-p), significantly exceeding the threshold for the development of cavitation in water, which is 4–5  $\mu\text{m}$  (p-p) [9]. The acoustic power was measured by the calorimetric method, and the results showed that the acoustic power was 120 W for the present experimental condition. The sonotrode served also as a grounded electrode. The tungsten high-voltage electrode was positioned at a distance of 4 mm from the grounded one.

A direct current power source (HAR-40P7.5-LN, Matsusada, Japan) with a maximum voltage of +40 kV and output power of 300 W was applied to charge a 1000 pF ceramic capacitor. The capacitor was then discharged in water through the above electrode system, thereby generating pulses into the solution as shown in Figure 1.

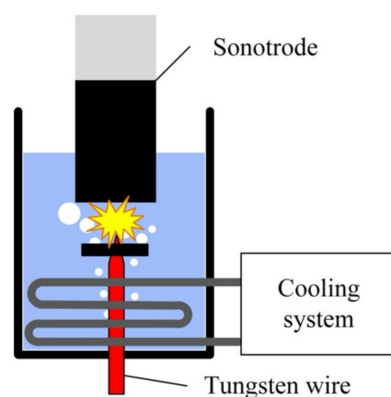


**Figure 1.** Schematic drawing of the treatment using a square iron plate.

Voltage between the electrodes was measured using an oscilloscope connected to the circuit through a 1000:1 reduction ratio high-voltage probe (PINTEC, Beijing, China), while the current signal was collected using a coil current probe (IWATSU, Tokyo, Japan). Additionally, several experiments were conducted using HPLC-TOFMS (high performance liquid chromatography time-of-flight mass spectrometry) to analyze the possible chemical reagents present in the solutions. The concentrations of *RhB* and  $\text{H}_2\text{O}_2$  were measured using a spectrophotometer (UV-VIS) as mentioned above.

Fenton reagents were introduced into the *RhB*-containing water bath through the following three routes: The first one was the addition of  $\text{Fe}^{2+}$  ions directly using an  $\text{FeCl}_2$  solution, as mentioned above. The second and third routes were the use of steel or iron parts immersed in the water bath. In the first case, a square iron plate (45 mm  $\times$  45 mm, thickness: 3 mm) was placed under the sonotrode tip, as shown in Figure 1. In the second case, the titanium tip of the sonotrode was replaced by a stainless-steel tip.

## 2.2. Experimental Conditions

The volume of treated solution was 2 liters. The solution conductivity was adjusted to 100  $\mu\text{S}/\text{cm}$  using the appropriate NaCl solution according to previous research [9]. The initial concentration of *RhB* was set to 5 mg/L. All solutions were prepared using ion exchanged water. During the experiment, argon gas was injected into the solution at a rate of 8 L/min through a porous plug. The porous plug was placed at the vessel bottom to facilitate the formation of fine bubbles in large quantities.

In order to achieve the optimal reaction conditions for *RhB* decomposition in the ACAP process assisted by Fenton reactions, experiments were conducted under various values of pH (3.5, 4.0, or 5.0), and concentrations of  $\text{FeCl}_2$  ranged from 3.5 to 20.0 mg/L. The duration of *RhB* decomposition treatment was 12 min in all experiments for purposes of comparing the results with our previous experiments, and the solution samples were taken at 3 min intervals. The vessel was cleaned with purified water before and after each experiment in order to remove residues of *RhB* that might have remained from previous experiments. To eliminate the possible influence of light on the decomposition efficiency, the experiments were done in total darkness.

The concentration of Fe ion was measured by ICPS-8100 (ICP Emission Spectroscopy). The concentration of *RhB* in the sample solutions was determined by absorbance spectroscopy at a wavelength of 554 nm using a spectrophotometer (UV-VIS). The efficiency of *RhB* decomposition ( $\eta$ ) was calculated by using the following equation:

$$\eta = \frac{\{[RhB]_o - [RhB]\}}{[RhB]_o} \times 100\% \quad (1)$$

where  $[RhB]_o$  is the initial concentration of *RhB*, and the  $[RhB]$  is the current concentration of *RhB* in the sample after treatment.

### 2.3. Methods for Measuring $\text{H}_2\text{O}_2$ Concentration

It is well known that the concentration of  $\text{H}_2\text{O}_2$  is a key parameter influencing the Fenton and Fenton-like reactions. Thus, in the current experiments, it was of crucial importance to measure the  $\text{H}_2\text{O}_2$  concentration. The measurements were done by the referenced method [15] with the help of UV-VIS spectrophotometry. Specifically, a mixture of 0.40 M potassium iodide, 0.06 M sodium hydroxide, and 0.10 mM ammonium molybdate was added to 0.10 M phthalic acid for a total volume of 0.75 mL. Then 1.5 mL of *RhB* solution was added to the mixture, and, after standing for 2 min, the solution absorbance was measured at a wavelength of 352 nm. The calibration curve for  $\text{H}_2\text{O}_2$  was plotted by measuring the absorbance under the same conditions by mixing 0.75 mL of the detection reagent with 1.5 mL of  $\text{H}_2\text{O}_2$  at standard concentrations ranging from 0 to 10 mg/L. Furthermore, the calibration data were fitted by the following formula:

$$y = 0.382 \times x + 0.018 \quad (2)$$

where  $x$  is the  $\text{H}_2\text{O}_2$  concentration, and  $y$  is the absorbance at 352 nm.

Preliminary experiments showed that the *RhB* solution had a non-zero absorbance at 352 nm that might have influenced the measurement results, especially when the  $\text{H}_2\text{O}_2$  concentration was small. Therefore, the following procedure was used to measure the  $\text{H}_2\text{O}_2$  concentration properly: First, a sample of solution was taken to measure the absorbance at a wavelength of 352 nm, and its value is denoted by  $y_1$  in Equation (3). The detection reagent was then added to the solution, and its absorbance  $y_2$  was measured again. The absorbance of  $\text{H}_2\text{O}_2$ ,  $y$ , was calculated according to the following equation:

$$y = y_1 - 1/2 \times y_2 \quad (3)$$

The value of  $y_2$  was divided by 2, because the *RhB* concentration in solution for measuring  $y_1$  was half that for measuring  $y_2$ .

## 3. Results

Using the above experimental methods and equipment, we measured the concentration of *RhB* under different conditions. Below is an explanation of the experimental results.

### 3.1. Effect of Temperature and FeCl<sub>2</sub> Addition on Decomposition Efficiency

Temperature can have a significant influence on the kinetics of *RhB* degradation. However, our preliminary experiments showed that the decomposition efficiency did not depend on whether the water temperature was controlled or not. In these experiments, a water-cooling coil was installed inside the ACAP reactor, and the *RhB* treatment was carried out with and without water cooling. The conditions and results are presented in Table 1. The reason why the temperature control did not have any effect on the treatment efficiency is assumed to be as follows: In the experiments, both the ultrasound irradiation and plasma discharge caused heat evolution into the inter-electrode zone, and then the heat increased throughout the whole bath. However, the temperature was distributed very non-uniformly, being highest near the electrodes and much lower away from them. All reactions involved in the *RhB* decomposition took place in the inter-electrode zone, the temperature of which can be very high and unaffected by the presence of the water-cooling coil. Based on these findings, all experiments in the present study were performed without controlling the water bath temperature.

**Table 1.** Effect of temperature on *RhB* decomposition efficiency at pH 4 and FeCl<sub>2</sub> 5 mg/L.

	Temperature (°C)	<i>RhB</i> Decomposition Efficiency (%)
With temperature control	20	77.7
Without temperature control	20–40	77.3

Figure 2 shows the effects of Fe<sup>2+</sup> addition on the *RhB* decomposition efficiency. Obviously, all Fe<sup>2+</sup> ions were supplied by FeCl<sub>2</sub>. As can be seen, the amount of Fe<sup>2+</sup> added had a great influence on the decomposition efficiency in the range of 0–5 mg/L FeCl<sub>2</sub> addition, where it increased from approximately 60% to 80%. These results suggest that the Fenton reactions had a great enhancing effect on the *RhB* decomposition efficiency. However, as the FeCl<sub>2</sub> addition further increased, the decomposition efficiency remained unchanged or even slightly decreased. As will be shown later, the reason for this is a limitation of H<sub>2</sub>O<sub>2</sub> generated in the plasma and cavitation zone.

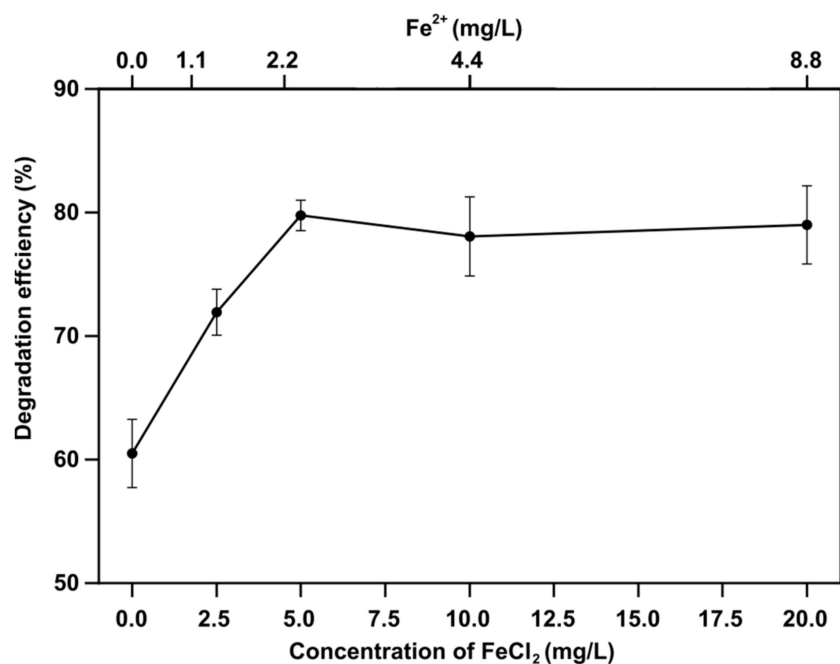


**Figure 2.** Effect of FeCl<sub>2</sub> concentration on decomposition efficiency at pH 4.

### 3.2. Effect of Initial pH Level on Decomposition Efficiency

The pH value is an important parameter for the Fenton reactions, and it has been reported that the optimum pH is around 2–5 [16,17]. We conducted experiments using 5 mg/L  $\text{FeCl}_2$  solutions in the presence of ultrasonic cavitation and plasma at different initial pH values. The results revealed that the effect of  $\text{FeCl}_2$  addition on the decomposition efficiency is pH-dependent. Figure 3 compares time variations of the decomposition efficiency at various pH values. It is clearly seen that the efficiency remained the same at pH = 4.0 and 3.5, reaching 80%. However, it decreased to 60% with increases in the pH value to 5.0. It should be mentioned that 3.5 was the minimum pH value that could be reached under the given conditions [9]. Thus, this result indicates that lower pH levels would be beneficial to achieve better decomposition efficiency. Chang [18] also reported similar results. In his study, the Fenton reactions were used to decolorize the *RhB* in aqueous solution at pH 2, 3, 4, and 5. The results indicated that higher *RhB* decomposition efficiency (>90%) could be obtained at pH 2, 3, and 4 compared to 66% at pH 5 after 30 min reaction time. As is well known, *RhB* is a type of cationic dye, and hence its decomposition rate should be higher at lower pH values. However, according to the results of our previous research [9], a decrease in pH results in an increase in electrical conductivity of the solution, which has a negative effect on the plasma discharge efficiency in the ACAP process. Therefore, based on the above results, pH 4.0 was considered the best value under the given experimental conditions.

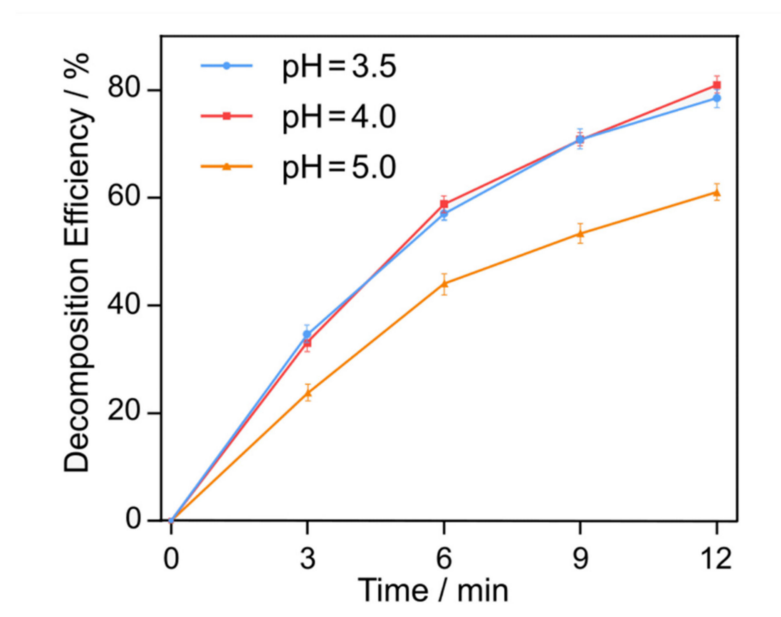
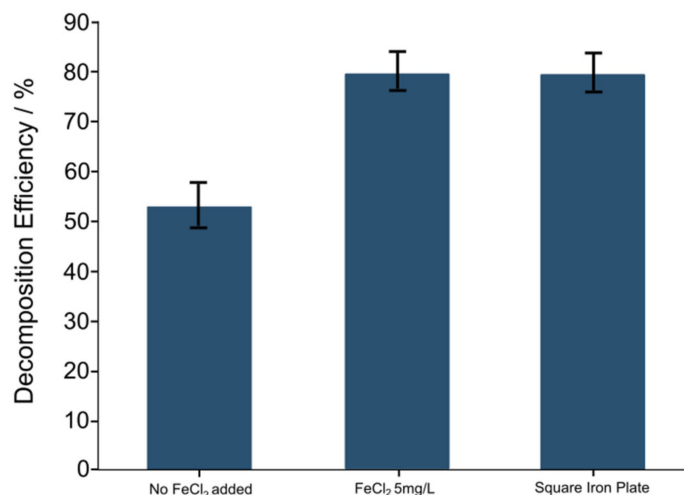


Figure 3. Time variation of *RhB* decomposition efficiency at various pH values.

### 3.3. Decomposition Efficiency in the Presence of Steel Parts

The above results thus revealed that the *RhB* decomposition efficiency became greater in the presence of  $\text{Fe}^{2+}$  ions in solution due to Fenton reactions. Furthermore, a very small amount of  $\text{Fe}^{2+}$  ions was needed to enhance the degradation efficiency of *RhB* in the present conditions. Hence, it will be interesting to examine the possibility of obtaining a similar effect due to  $\text{Fe}^{2+}$  ions entering into the solution from steel parts of the ACAP reactor. Obviously, such an option would be beneficial in terms of preventing secondary pollution and increasing the economic efficiency. Therefore, we conducted experiments using a square iron plate placed under the sonotrode, as shown in Figure 1. The experiments were performed under exactly the same experimental conditions (vibration amplitude, frequency, reactor design, and so on). Therefore, we assure that the sonochemical activity was also the same. Figure 4 compares the *RhB* degradation efficiency obtained under different experimental conditions. It can be seen that in the presence of the iron plate, the

*RhB* decomposition efficiency increased to approximately 76% versus 53% without the plate after 12 min of treatment. However, the decomposition efficiency with the iron plate was still lower than the maximum value of 80% obtained at the 5 mg/L concentration of  $\text{FeCl}_2$ . Additional measurements revealed that the concentration of ferrous ions after 12 min treatment was 1.73 mg/L. This was slightly lower than the concentration of iron ions in 5 mg/L  $\text{FeCl}_2$ , which was 2.21 mg/L of ferrous ion. This indicated that iron ions dissolved from the iron plates during the ACAP treatment, and that Fenton reactions occurred, promoting the decomposition of *RhB*. Therefore, placing iron or steel components in the ACAP reactor can also improve the efficiency of *RhB* decomposition, producing almost the same effect as adding ferrous ions.



**Figure 4.** The *RhB* decomposition efficiency under different conditions at pH = 4.

Next, the sonotrode with a titanium tip was replaced by a sonotrode with a stainless-steel tip. This stainless steel was composed of 18% Cr and 10% Ni, and the balance was Fe. The experiments were carried out under the same conditions, and the results are presented in Figure 5. It can be seen from this figure that the *RhB* decomposition efficiency was slightly higher in the experiments with a stainless steel tip as compared to the titanium tip case. This difference was especially noticeable at pH 3.5 and 5. However, the effect of using a stainless steel sonotrode was not as good as that of placing iron plates. At pH 3.5, when a stainless steel sonotrode was used, the *RhB* decomposition efficiency was highest, at 63%. However, it was lower than the *RhB* decomposition efficiency of 76% when the iron plate was used. Therefore, it is more effective to place the iron plate under the titanium sonotrode tip than to change it for the stainless steel sonotrode tip.

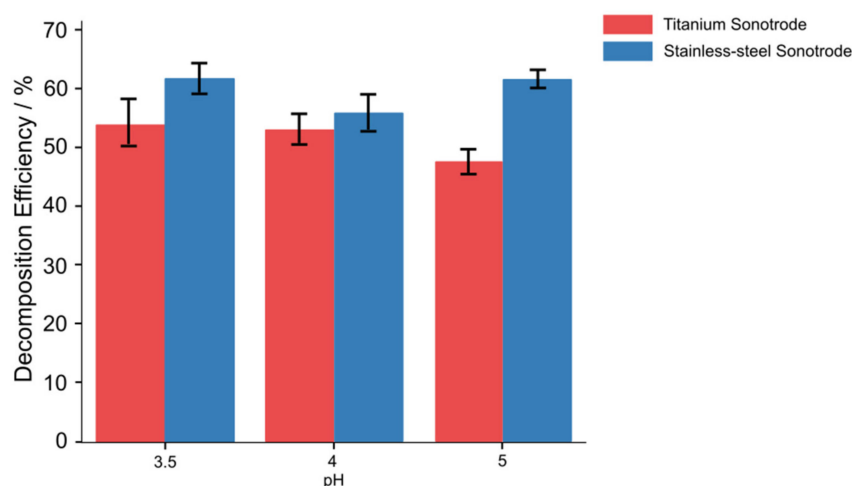


**Figure 5.** The *RhB* decomposition efficiency with different sonotrodes.

Thus, it can be concluded from the above results that iron or steel parts of the experimental setup can additionally improve the efficiency of *RhB* degradation. Details and possible mechanisms will be discussed in the following section.

#### 4. Discussion

The above experimental results show that the efficiency of *RhB* decomposition is definitely affected by Fenton reactions. Moreover, Fenton reagents can be supplied not only by the addition of iron salts but also from parts of the experimental reactor used in the study. The following section focuses on explanations for possible mechanisms of *RhB* decomposition

##### 4.1. Possible Chemical Reactions with $FeCl_2$ Addition

Some basic reactions and mechanisms, which are responsible for the decomposition of rhodamine B, were discussed in our previous papers [8–10]. However, as the presence of iron ions in the system makes the relevant chemical reactions more complicated, some typical and important reactions are considered in more detail below.

The first group of reactions involves highly active chemical radicals that are generated due to ultrasonic cavitation and plasma discharge. Ultrasound irradiation in liquids is known to cause acoustic cavitation, whereby the formation, growth, and implosion of bubbles filled with gas and/or vapor takes place. The cavities that are formed oscillate in cycles of ultrasound wave expansion and contraction [19]. The pressure and the temperature in the cavitation bubbles can reach several hundred atmospheres and several thousand degrees K as the bubbles collapse following explosion [20]. Hydroxyl radicals form under these conditions due to a number of phenomena, including water sonolysis, hot particle collision, and formation of a plasma within the cavitation bubbles [21]. The radicals subsequently participate in a variety of reactions inside a gas bubble and/or in the bulk solution itself. Equations (4)–(8) show some typical reactions. [20]:



In plasma-assisted processes, energetic electrons can interact with other molecules such as  $O_2$  and  $H_2O$ , thereby producing various reactive species that include  $HO\cdot$  and  $O_2^{\cdot-}$ , but also reactive molecules such as  $O_3$  and  $H_2O_2$ . Furthermore, photogenerated holes ( $h^+$ ) and photo-generated electrons ( $e^-$ ) can participate in catalytic redox reactions, producing  $H_2O_2$  and dissolved oxygen [22].

In the case of argon injection, whereas argon is not involved in the chemical reaction, it assists plasma generation by lowering the underwater dielectric breakdown voltage and by raising the temperature in the ultrasonic cavitation zone. As a result of these phenomena, more chemically active hydrogen and oxygen-containing ions and radicals are generated when argon is introduced into the reactor. This was found to further promote *RhB* decomposition [10].

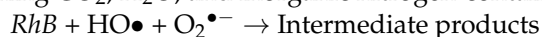
The second group of reactions comprises the Fenton reactions, which involve hydrogen peroxide and iron ions,  $Fe^{2+}$  and  $Fe^{3+}$ . The commonly accepted mechanism of the Fenton reactions is represented by Equations (9)–(12), and the reaction rate constants,  $k$ , can be found in the relevant literature [23]. The Fenton reaction itself is considered to be the reaction represented by Equation (9). This encompasses the oxidation of ferrous to ferric ions that decompose hydrogen peroxide into the hydroxyl radical and the hydroxide

ion. The core of Fenton reaction chemistry is typically considered to be reaction (9), but reactions (10)–(12) must also be taken into account as needed for the entire reaction path:



The ferric ions generated are reduced by reacting with excess hydrogen peroxide, again forming ferrous ion and other radicals based on reaction (10). This reaction is called the Fenton-like reaction, and it allows  $\text{Fe}^{2+}$  regeneration in an effective cyclic mechanism. It is seen that the reaction rate constant (10) is much lower than that of Fenton reaction (9). In the Fenton-like reaction, apart from ferrous ion regeneration, the hydroperoxyl radical  $\text{HO}_2\bullet$  is also produced, which can also attack organic contaminants.

Subsequently, highly active radicals  $\text{HO}\bullet$  and  $\text{O}_2^{\bullet-}$  react with *RhB* molecules to generate a variety of intermediate species, followed by *RhB* being entirely mineralized, thereby forming  $\text{CO}_2$ ,  $\text{H}_2\text{O}$ , and inorganic nitrogen-containing ions as per Equation (13).



Thus, in the ACAP process there are a number of physical and chemical phenomena resulting in the generation of chemically active radicals and free electrons that contribute to the decomposition of rhodamine B in aqueous solution. Among them, the Fenton reaction plays an important auxiliary role in the degradation process, because it allows hydrogen peroxide to convert back into hydroxy radicals. Nevertheless, in the present experimental conditions, the capacity of the Fenton reactions to improve decomposition efficiency was limited, as follows from Figures 2–5. Furthermore, due to the limited processing time (12 min) in our experiments, the maximum processing efficiency that *RhB* can achieve was 80%. If the *RhB* solution is to be completely decomposed into carbon dioxide and water, the treatment time needs to be increased. Below is one possible explanation of the reasons and underlying mechanisms.

#### 4.2. Production of Hydrogen Peroxide in the ACAP Reactor

The concentration of hydrogen peroxide plays a crucial role in deciding the overall efficiency of the decomposition process. In order to evaluate the hydrogen peroxide production in the ACAP process using Fenton reactions, the  $\text{H}_2\text{O}_2$  concentration was measured with a UV–VIS spectrophotometer, as mentioned in the previous section. The measurement results are shown in Figure 6. As mentioned above, both the acoustic cavitation and underwater plasma can generate hydroxyl radical  $\text{HO}\bullet$ , a portion of which can react with each other and thus further generate hydrogen. The reaction details are presented in Section 4.1.

As illustrated in Figure 6, the  $\text{H}_2\text{O}_2$  concentration and its time variation are significantly dependent on the amount of  $\text{FeCl}_2$  added. Without  $\text{FeCl}_2$  addition, the  $\text{H}_2\text{O}_2$  concentration continuously rises. This is because the rate of  $\text{H}_2\text{O}_2$  self-decomposition is much slower than its production rate [24]. However, when  $\text{FeCl}_2$  was added to the solution, the concentration of hydrogen peroxide slowly increased during the first 6–9 min of treatment and then started to decrease with time. In general, this time variation in  $\text{H}_2\text{O}_2$  concentration becomes smaller as the amount of  $\text{FeCl}_2$  addition increases. These results suggest that  $\text{H}_2\text{O}_2$  is consumed by the Fenton reactions, especially by reaction (9), because it proceeds much faster than reaction (10). As shown in Figure 2, the efficiency of *RhB* degradation was drastically increased first and then kept almost unchanged when the amount of  $\text{FeCl}_2$  added exceeded 5 mg/L. These results, when considered together,

indicate that the Fenton reactions were ongoing, and that the production and consumption of hydrogen peroxide were in dynamic equilibrium in the solution. When the concentration of  $\text{FeCl}_2$  was increased from 0 to 5 mg/L, the concentration of hydrogen peroxide gradually decreased, but when the concentration of  $\text{FeCl}_2$  was higher than 5 mg/L, the concentration of hydrogen peroxide in the solution remained almost constant. This is because the hydrogen peroxide was consumed by  $\text{Fe}^{2+}$  ions in the Fenton reactions, and the greater the amount of  $\text{FeCl}_2$  was added, the lower the concentration of hydrogen peroxide. However, when the amount of  $\text{FeCl}_2$  added exceeded 10 mg/L, the differences between the  $\text{H}_2\text{O}_2$  concentrations became insignificant. This can be readily seen from a comparison of  $\text{H}_2\text{O}_2$  concentration time variations for  $\text{FeCl}_2$  addition of 10 and 20 mg/L. Moreover, the  $\text{H}_2\text{O}_2$  concentration itself becomes close to the limit of measurement accuracy of the analysis. Thus, results suggest that the efficiency enhancement effect of  $\text{Fe}^{2+}$  ion addition is limited by the generation rate of  $\text{H}_2\text{O}_2$  in the cavitation-plasma zone. That is why the *RhB* decomposition efficiency first increases with the addition of  $\text{FeCl}_2$  and then remains almost constant with further addition, as shown in Figure 2.

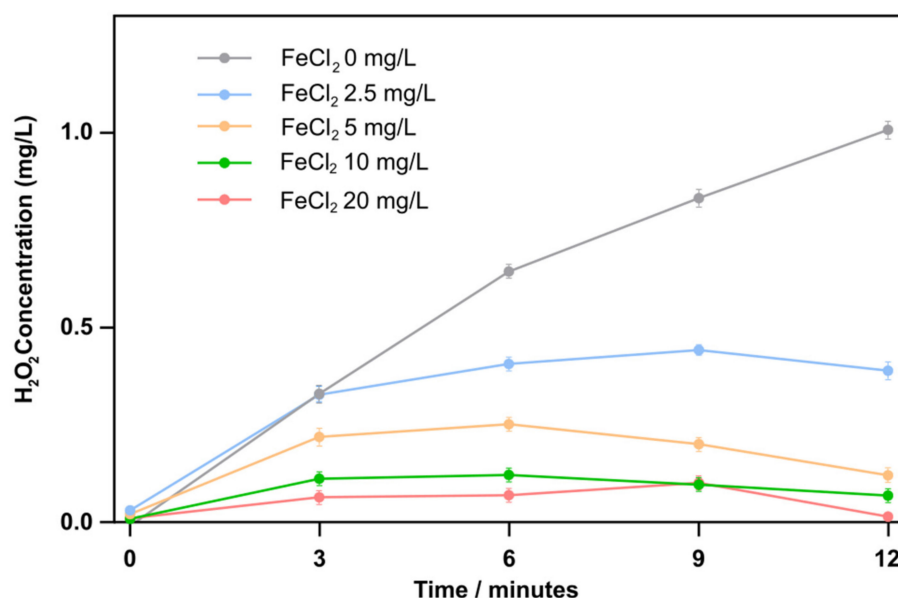


Figure 6. Time variation of  $\text{H}_2\text{O}_2$  concentration at pH = 4 with different amounts of  $\text{FeCl}_2$  addition.

However, when  $\text{Fe}^{2+}$  ions are supplied to the *RhB* solution from the solid surfaces such as the iron plate or the steel sonotrode tip, the additional effect of Fenton reactions is controlled by the dissolution rate of these iron-containing solid surfaces. The results suggest that this dissolution rate is rather slow and depends on the solution pH. Another technique that can potentially enhance the iron dissolution rate is an increase in the surface area of the iron-containing part contacting the liquid bath. This issue should be properly investigated in further studies.

#### 4.3. Mechanisms of *RhB* Decomposition

Based on the above discussion, a plausible mechanism for rhodamine B decomposition was considered. One mechanism is illustrated in Figure 7. It should be noted that the decomposition process is very complex and involves several parallel and consecutive reactions. First, as mentioned above, active radicals such  $\text{HO}\bullet$ ,  $\text{H}\bullet$ , and  $\text{HO}_2\bullet$  are produced according to the following three pathways: (1) sonolysis reaction; (2) water pyrolysis during the plasma discharge; (3) and Fenton and Fenton-like reactions.

The first two mechanisms are considered to be the main contributors to the production of  $\text{HO}\bullet$  radicals, the greater part of which attacks *RhB* molecules, causing their decomposition. Thus, the *RhB* decomposition proceeds mainly according to the first and second pathways. Nevertheless, some proportion of  $\text{HO}\bullet$  radicals can recombine to produce  $\text{H}_2\text{O}_2$

according to reaction (7), and this hydrogen peroxide is assumed to serve as a reagent in the Fenton reactions, as discussed above.

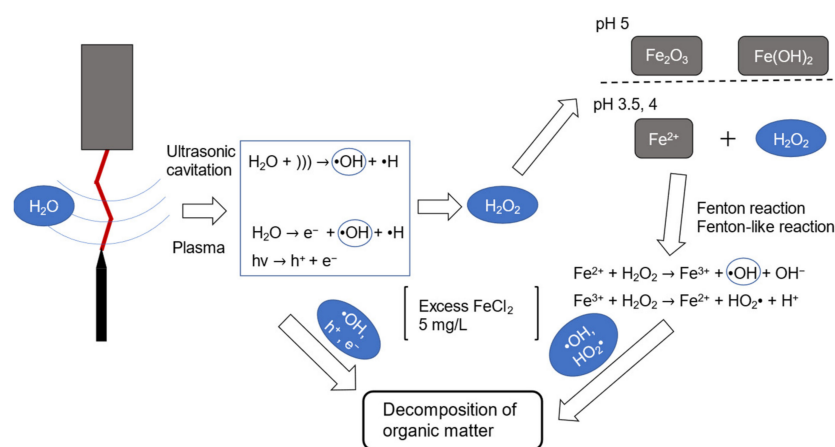


Figure 7. Possible mechanisms of rhodamine B decomposition.

Finally, it is important to identify possible intermediate products formed during the reactions leading to *RhB* decomposition. The identification was made by liquid chromatography, as mentioned above. Samples were taken after 15 min and 30 min treatment times, the results are shown in Appendix A. The proposed decomposition pathway of *RhB* is shown in Figure 8.

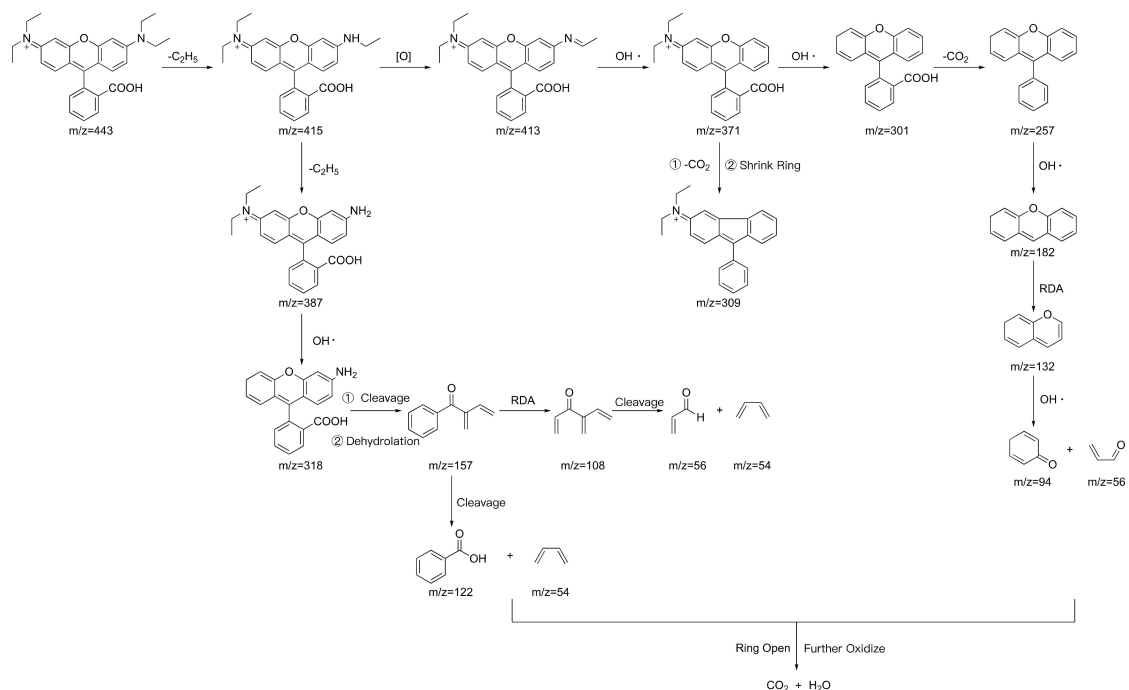


Figure 8. Proposed decomposition pathways of *RhB* in the ACAP/Fenton treatment process.

Major intermediates, which form during the degradation process, were thus identified based on the  $m/z$  values of the mass spectra, taking into account results in the relevant literature [25–27]. As shown in Figure 8, active species such as OH are generated in the ACAP treatment process. The OH radical affects the entire degradation process. Moreover, the intermediates are further decomposed into small molecular intermediates, including organic acids, by cleavage of conjugated structures that are finally oxidized into  $\text{CO}_2$  and  $\text{H}_2\text{O}$ .

#### 4.4. Reaction Kinetics and Comparison of Various Treatment Methods

In order to clarify the kinetics of the *RhB* decomposition reaction in the Fenton-assisted ACAP process, the experimental results of the decomposition of *RhB* were fitted using a first order kinetics model [28]. The *RhB* decomposition kinetics can thus be written as follows:

$$\ln \frac{[C]_0}{[C]} = kt \quad (14)$$

where  $[C]_0$  is the initial concentration of *RhB*,  $[C]$  is the concentration of *RhB* at time  $t$ , and  $k$  is the first-order decomposition rate constant ( $\text{min}^{-1}$ ).

The fitting kinetic curves and corresponding calculated kinetic constants are presented in Figure 9 for a number of typical measurements. It can be seen that the dots fall more or less on straight lines, suggesting the first order kinetics of *RhB* decomposition under the given experimental conditions. The first-order kinetic rate constants of *RhB* decomposition were  $0.129 \text{ min}^{-1}$  and  $0.115 \text{ min}^{-1}$  in the ACAP process with the  $5 \text{ mg/L}$  addition of  $\text{FeCl}_2$  and with the iron plate, versus  $0.060 \text{ min}^{-1}$  when the ACAP treatment was carried out without Fenton reactions. In addition, we compared our results with other data reported for the *RhB* decomposition in the literature. The results are summarized in Figure 10 and indicate that the ACAP with  $\text{FeCl}_2$  added, and with the iron plate in place, both possessed an improved promoting effect on *RhB* decomposition.

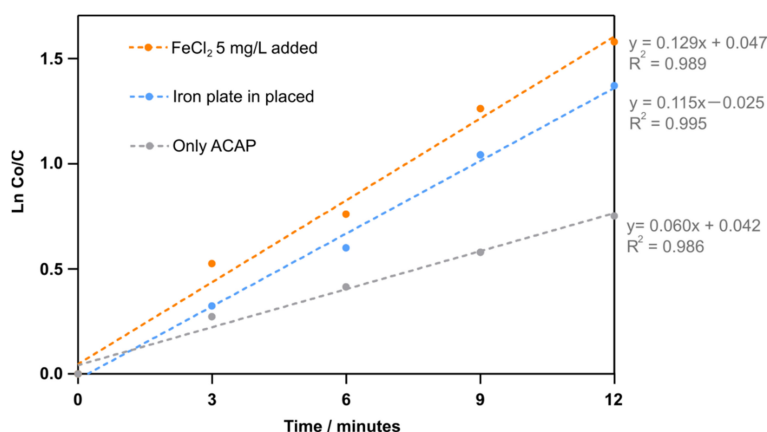


Figure 9. Time variation of dimensionless *RhB* concentration under different treatment conditions.

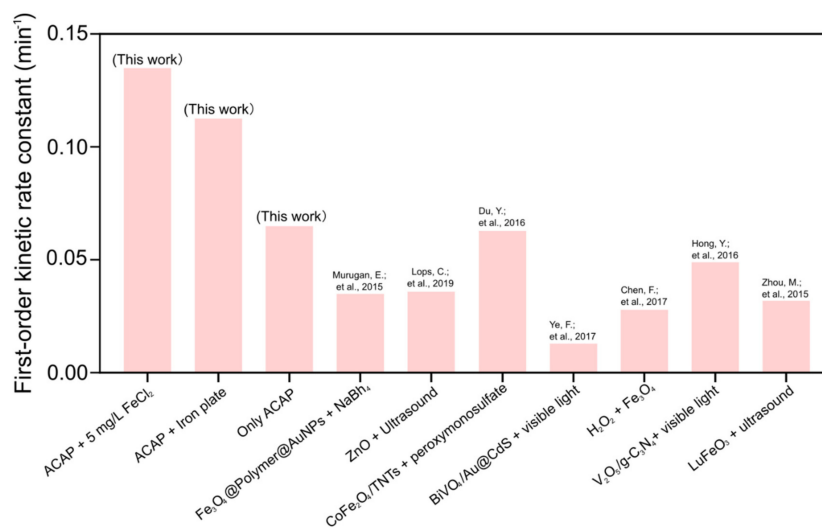


Figure 10. Comparison of the first order kinetics rate constants obtained in the present and other studies of *RhB* decomposition [29–35].

## 5. Conclusions

In this study, in order to further improve wastewater treatment efficiency, we investigated the promoting effects of Fenton reactions on the decomposition efficiency of rhodamine B in aqueous solution treated by the ACAP process, which was recently proposed by the authors here. Two options for ferrous ion supply were considered: one was addition of  $\text{FeCl}_2$ , and the other was dissolution of iron from parts of the ACAP reactor into the *RhB*-containing solution. To investigate the plausible reaction mechanisms, the hydrogen peroxide concentration was measured under different experimental conditions. Additionally, rhodamine B and its decomposition intermediates were analyzed by the HPLC-TOFMS method to predict possible decomposition pathways of *RhB*. The results of the present study are summarized as follows:

- (1) The Fenton reactions greatly enhanced the efficiency of the acoustic cavitation-assisted plasma decomposition of rhodamine B. Under the present experimental conditions, the decomposition efficiency reached almost 80%, which is 20% greater compared to the case without Fenton reactions.
- (2) When  $\text{FeCl}_2$  was added to the solution, the *RhB* decomposition efficiency was affected by the pH and the concentration of  $\text{Fe}^{2+}$  ions. At  $\text{pH} = 4$ , the degradation efficiency increased up to 80% as the amount of added  $\text{FeCl}_2$  increased from 0 to 5 mg/L, and then it remained approximately at the same level with further addition of  $\text{FeCl}_2$ .
- (3) Placing iron or steel components inside the ACAP reactor could also improve the efficiency of *RhB* decomposition, although the effect was slightly less than in the case of ferrous ion addition, due to the slow dissolution rate of steel parts in the aqueous solution.
- (4) The mechanism of enhanced Fenton-assisted degradation of *RhB* is suggested to be as follows: ultrasonic cavitation and plasma discharge generate  $\text{HO}\bullet$  radicals but a portion recombines to produce  $\text{H}_2\text{O}_2$ , which reacts with  $\text{Fe}^{2+}$  ions to produce  $\text{HO}\bullet$  radicals again. Under the present experimental conditions, a 5 mg/L addition of  $\text{FeCl}_2$  was sufficient to convert all  $\text{H}_2\text{O}_2$  to the hydroxyl radicals.
- (5) The first order kinetics rate constants of *RhB* decomposition obtained in our experiments were compared with other studies. The results indicated that the ACAP with  $\text{FeCl}_2$  5 mg/L added to solution directly or with an iron plate installed under the sonotrode tip both had an enhanced promoting effect on *RhB* decomposition.

**Author Contributions:** Conceptualization, S.K., T.Y. and Y.X.; methodology, S.K. and Y.X.; software, Y.X. and T.K.; validation, Y.X. and T.K.; formal analysis, Y.X. and T.K.; investigation, Y.X. and T.K.; resources, Y.X.; data curation, Y.X. and T.K.; writing—original draft preparation, Y.X.; writing—review and editing, S.K. and Y.X.; visualization, Y.X. and T.K.; supervision, S.K. and T.Y.; project administration, S.K. and T.Y.; funding acquisition, S.K. and T.Y. All authors have read and agreed to the published version of the manuscript.

**Funding:** This research was funded by the China Scholarship Council, CSC201908420297.

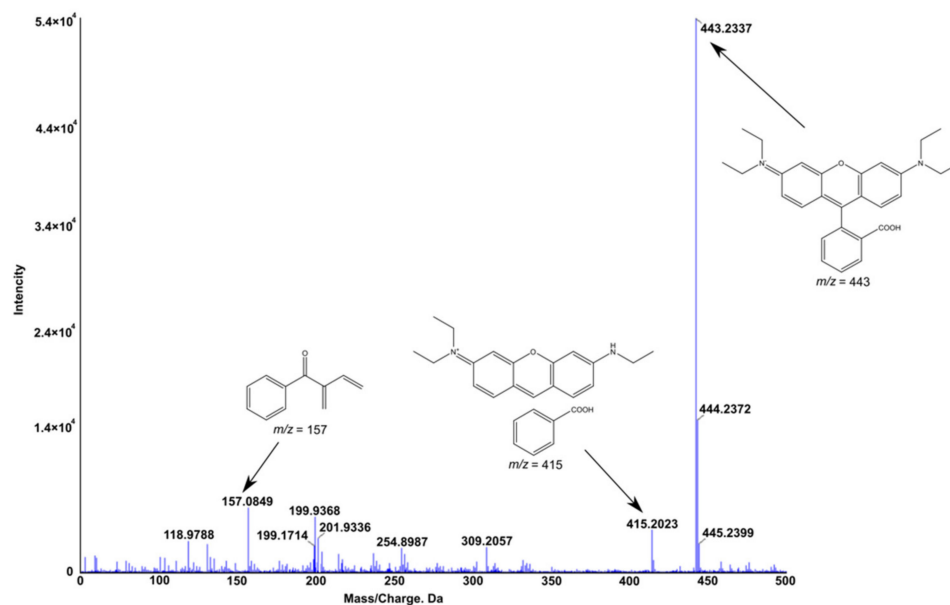
**Data Availability Statement:** The data presented in this study are available in article.

**Conflicts of Interest:** The authors declare no conflict of interest.

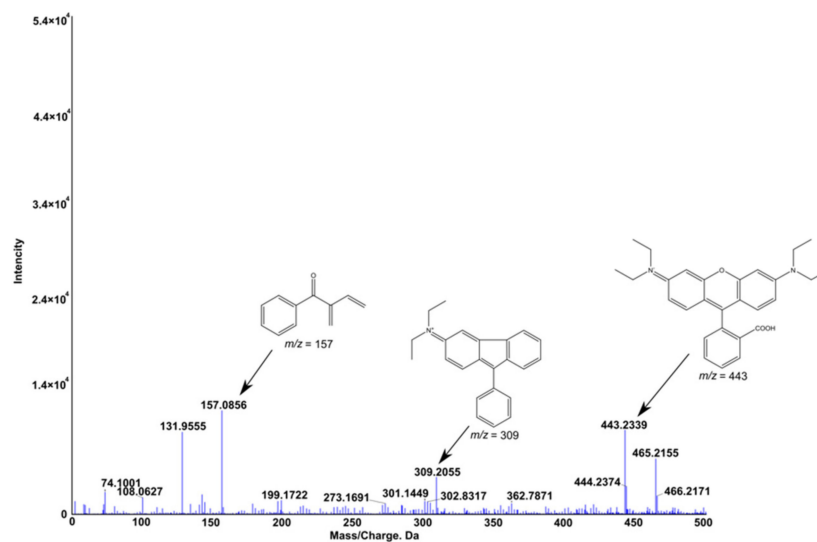
## Appendix A

The HPLC test results are shown in the following figures. Figure A1 shows the mass spectra of the treated solutions at different treatment times. Based on the comparison of mass spectra, we excluded some background and impurity ions, peaks at  $m/z = 59, 101,$  and  $187,$  and so on. From the mass spectra, it was clearly revealed that the  $m/z$  value of 443 corresponded to *RhB*, and fragments with  $m/z$  values of 415 and 387 were those of N-de-ethylated intermediates of *RhB*. The product of  $m/z$  309 and 318 contributed to hydroxyl radical (OH) attack of the double bonds to cause ring opening reaction. Further decomposition by radical attack on the conjugated xanthene ring led to formation of smaller fragments, such as an intermediate with an  $m/z$  value of 157, and other low molecular

weight intermediates, as shown in Figure 8. As the treatment time increased, the intensity of *RhB* gradually decreased, and when the treatment time was 30 min, it was found that the intensity of *RhB* was very low, from which it could be inferred that after 30 min of treatment, *RhB* was broken down into small molecules, which were eventually decomposed into CO<sub>2</sub> and H<sub>2</sub>O.



(a) 0 min



(b) 15 min

Figure A1. Cont.

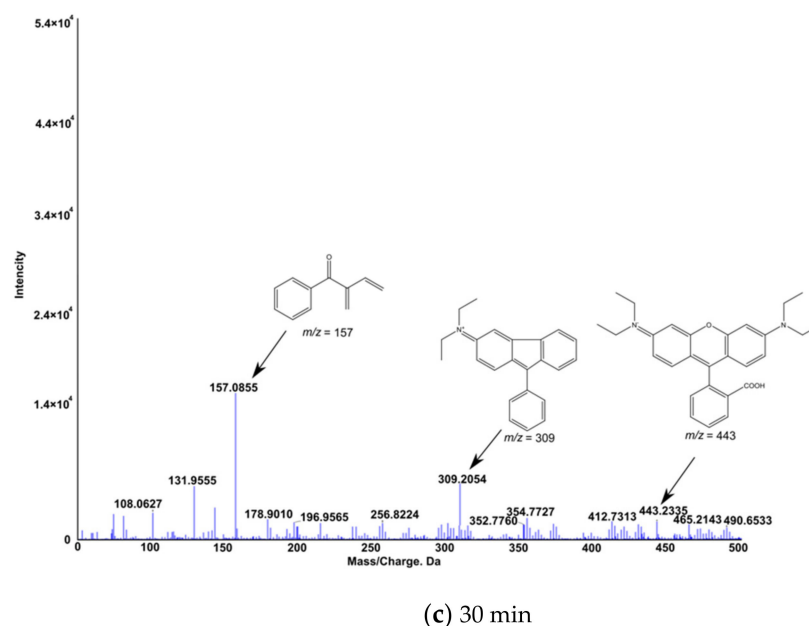


**Figure A1.** Mass spectra of the treated solutions at different treatment times: (a) initial, (b) 15 min, and (c) 30 min.

## References

- Vanraes, P.; Nikiforov, A.Y.; Leys, C. Electrical discharge in water treatment technology for micropollutant decomposition. In *Plasma Science and Technology—Progress in Physical States and Chemical Reactions*; IntechOpen: London, UK, 2016; pp. 428–478.
- Stratton, G.R.; Dai, F.; Bellona, C.L.; Holsen, T.M.; Dickenson, E.R.; Mededovic Thagard, S. Plasma-based water treatment: Efficient transformation of perfluoroalkyl substances in prepared solutions and contaminated groundwater. *Environ. Sci. Technol.* **2017**, *51*, 1643–1648. [[CrossRef](#)] [[PubMed](#)]
- Stratton, G.R.; Bellona, C.L.; Dai, F.; Holsen, T.M.; Thagard, S.M. Plasma-based water treatment: Conception and application of a new general principle for reactor design. *Chem. Eng. J.* **2015**, *273*, 543–550. [[CrossRef](#)]
- Shen, Y.; Lei, L.; Zhang, X.; Zhou, M.; Zhang, Y. Improvement of diagnostic techniques and electrical circuit in azo dye degradation by high voltage electrical discharge. *Energy Convers. Manag.* **2008**, *49*, 2254–2263. [[CrossRef](#)]
- Sato, M. Degradation of organic contaminants in water by plasma. *Int. J. Plasma Environ. Sci. Technol.* **2009**, *3*, 8–14.
- Peng, J.; Wang, Z.; Wang, S.; Liu, J.; Zhang, Y.; Wang, B.; Gong, Z.; Wang, M.; Dong, H.; Cao, Z.; et al. Enhanced removal of methylparaben mediated by cobalt/carbon nanotubes (Co/CNTs) activated peroxymonosulfate in chloride-containing water: Reaction kinetics, mechanisms and pathways. *Chem. Eng. J.* **2021**, *409*, 128176. [[CrossRef](#)]
- Takahashi, T.; Takada, N.; Toyoda, H. 3p4–6 effect of superposing ultrasonic wave on microwave plasma under water. *Proc. Symp. Ultrason. Electron.* **2013**, *34*, 441–442.
- Komarov, S.; Yamamoto, T.; Fang, Y.; Hariu, D. Combined effect of acoustic cavitation and pulsed discharge plasma on wastewater treatment efficiency in a circulating reactor: A case study of rhodamine b. *Ultrason. Sonochem.* **2020**, *68*, 105236. [[CrossRef](#)]
- Fang, Y.; Hariu, D.; Yamamoto, T.; Komarov, S. Acoustic cavitation assisted plasma for wastewater treatment: Degradation of rhodamine b in aqueous solution. *Ultrason. Sonochem.* **2019**, *52*, 318–325. [[CrossRef](#)]
- Xu, Y.; Yamamoto, T.; Hariu, D.; Komarov, S. Effect of gas injection on cavitation-assisted plasma treatment efficiency of wastewater. *Ultrason. Sonochem.* **2022**, *83*, 105941. [[CrossRef](#)] [[PubMed](#)]
- Qi, C.; Wen, Y.; Zhao, Y.; Dai, Y.; Li, Y.; Xu, C.; Yang, S.; He, H. Enhanced degradation of organic contaminants by Fe (III)/peroxymonosulfate process with L-cysteine. *Chin. Chem. Lett.* **2022**, *33*, 2125–2128. [[CrossRef](#)]
- Dai, Y.; Qi, C.; Cao, H.; Wen, Y.; Zhao, Y.; Xu, C.; Yang, S.; He, H. Enhanced degradation of sulfamethoxazole by microwave-activated peracetic acid under alkaline condition: Influencing factors and mechanism. *Sep. Purif. Technol.* **2022**, *288*, 120716. [[CrossRef](#)]
- Pirsaheb, M.; Hossaini, H.; Raad, N.K.; Kianpour, S.; Hossini, H. A systematic review on photo-fenton process as an efficient advanced oxidation for degradation of amoxicillin in aqueous environments. *Rev. Environ. Health* **2022**. [[CrossRef](#)] [[PubMed](#)]
- Steinberg, S.M. High-performance liquid chromatography method for determination of hydrogen peroxide in aqueous solution and application to simulated martian soil and related materials. *Environ. Monit. Assess.* **2013**, *185*, 3749–3757. [[CrossRef](#)] [[PubMed](#)]
- Kormann, C.; Bahnemann, D.W.; Hoffmann, M.R. Photocatalytic production of hydrogen peroxides and organic peroxides in aqueous suspensions of titanium dioxide, zinc oxide, and desert sand. *Environ. Sci. Technol.* **1988**, *22*, 798–806. [[CrossRef](#)]

16. Ustün, G.E.; Solmaz, S.K.; Morsünbül, T.; Azak, H.S. Advanced oxidation and mineralization of 3-indole butyric acid (iba) by fenton and fenton-like processes. *J. Hazard. Mater.* **2010**, *180*, 508–513. [[CrossRef](#)]
17. Eary, L.E.; Rai, D. Chromate removal from aqueous wastes by reduction with ferrous ion. *Environ. Sci. Technol.* **1988**, *22*, 972–977. [[CrossRef](#)]
18. Chang, S.H.; Wang, K.S.; Li, H.C.; Wey, M.Y.; Chou, J.D. Enhancement of rhodamine b removal by low-cost fly ash sorption with fenton pre-oxidation. *J. Hazard. Mater.* **2009**, *172*, 1131–1136. [[CrossRef](#)] [[PubMed](#)]
19. Chowdhury, P.; Viraraghavan, T. Sonochemical degradation of chlorinated organic compounds, phenolic compounds and organic dyes—A review. *Sci. Total. Environ.* **2009**, *407*, 2474–2492. [[CrossRef](#)] [[PubMed](#)]
20. Babuponnusami, A.; Muthukumar, K. A review on fenton and improvements to the fenton process for wastewater treatment. *J. Environ. Chem. Eng.* **2014**, *2*, 557–572. [[CrossRef](#)]
21. Nikitenko, S.I.; Pflieger, R. Toward a new paradigm for sonochemistry: Short review on nonequilibrium plasma observations by means of MBSL spectroscopy in aqueous solutions. *Ultrason. Sonochemistry* **2017**, *35*, 623–630. [[CrossRef](#)] [[PubMed](#)]
22. Tao, X.; Yuan, X.; Huang, L.; Shang, S.; Xu, D. Fe-based metal-organic frameworks as heterogeneous catalysts for highly efficient degradation of wastewater in plasma/fenton-like systems. *RSC Adv.* **2020**, *10*, 36363–36370. [[CrossRef](#)] [[PubMed](#)]
23. Wahono, J.Z.; Yusharyahya, R.D.; Harianingsih; Saksono, N. Phenol degradation by fenton reaction in air injection using plasma electrolysis method. *IOP Conf. Ser. Mater. Sci. Eng.* **2020**, *980*, 012051. [[CrossRef](#)]
24. Ma, Y.; Chang, C.; Chao, C. Decolorization of rhodamine b by a photo-fenton process: Effect of system parameters and kinetic study. *Int. J. Environ. Resour.* **2012**, *1*, 73–80.
25. Natarajan, T.S.; Natarajan, K.; Bajaj, H.C.; Tayade, R.J. Enhanced photocatalytic activity of bismuth-doped tio2 nanotubes under direct sunlight irradiation for degradation of rhodamine b dye. *J. Nanopart. Res.* **2013**, *15*, 1669. [[CrossRef](#)]
26. Natarajan, T.S.; Thomas, M.; Natarajan, K.; Bajaj, H.C.; Tayade, R.J. Study on uv-led/tio2 process for degradation of rhodamine b dye. *Chem. Eng. J.* **2011**, *169*, 126–134. [[CrossRef](#)]
27. Ferreira, B.R.; Correa, D.N.; Eberlin, M.N.; Vendramini, P.H. Fragmentation reactions of rhodamine b and 6g as revealed by high accuracy orbitrap tandem mass spectrometry. *J. Braz. Chem. Soc.* **2017**, *28*, 136–142. [[CrossRef](#)]
28. Bai, Y.; Wu, D.; Wang, W.; Chen, P.; Tan, F.; Wang, X.; Qiao, X.; Wong, P.K. Dramatically enhanced degradation of recalcitrant organic contaminants in mgo(2)/fe(iii) fenton-like system by organic chelating agents. *Environ. Res.* **2021**, *192*, 110242. [[CrossRef](#)] [[PubMed](#)]
29. Zhou, M.; Yang, H.; Xian, T.; Li, R.S.; Zhang, H.M.; Wang, X.X. Sonocatalytic degradation of rhb over lufeo3 particles under ultrasonic irradiation. *J. Hazard. Mater.* **2015**, *289*, 149–157. [[CrossRef](#)] [[PubMed](#)]
30. Murugan, E.; Jebaranjitham, J.N. Dendrimer grafted core-shell fe3o4-polymer magnetic nanocomposites stabilized with aunps for enhanced catalytic degradation of rhodamine b—A kinetic study. *Chem. Eng. J.* **2015**, *259*, 266–276. [[CrossRef](#)]
31. Lops, C.; Ancona, A.; Di Cesare, K.; Dumontel, B.; Garino, N.; Canavese, G.; Hernández, S.; Cauda, V. Sonophotocatalytic degradation mechanisms of rhodamine b dye via radicals generation by micro- and nano-particles of zno. *Appl. Catal. B Environ.* **2019**, *243*, 629–640. [[CrossRef](#)] [[PubMed](#)]
32. Du, Y.; Ma, W.; Liu, P.; Zou, B.; Ma, J. Magnetic cofe2o4 nanoparticles supported on titanate nanotubes (cofe2o4/tnts) as a novel heterogeneous catalyst for peroxymonosulfate activation and degradation of organic pollutants. *J. Hazard. Mater.* **2016**, *308*, 58–66. [[CrossRef](#)] [[PubMed](#)]
33. Ye, F.; Li, H.; Yu, H.; Chen, S.; Quan, X. Constructing bivo4-au@cds photocatalyst with energetic charge-carrier-separation capacity derived from facet induction and z-scheme bridge for degradation of organic pollutants. *Appl. Catal. B Environ.* **2018**, *227*, 258–265. [[CrossRef](#)]
34. Chen, F.; Xie, S.; Huang, X.; Qiu, X. Ionothermal synthesis of fe(3)o(4) magnetic nanoparticles as efficient heterogeneous fenton-like catalysts for degradation of organic pollutants with h(2)o(2). *J. Hazard. Mater.* **2017**, *322*, 152–162. [[CrossRef](#)] [[PubMed](#)]
35. Hong, Y.; Jiang, Y.; Li, C.; Fan, W.; Yan, X.; Yan, M.; Shi, W. In-situ synthesis of direct solid-state z-scheme v2o5/g-c3n4 heterojunctions with enhanced visible light efficiency in photocatalytic degradation of pollutants. *Appl. Catal. B Environ.* **2016**, *180*, 663–673. [[CrossRef](#)]